Journal of Materials Chemistry C

ROYAL SOCIETY OF CHEMISTRY

PAPER

View Article Online
View Journal | View Issue

Cite this: J. Mater. Chem. C, 2023, 11, 11518

Substrate-dependent spin crossover in an Fe(II) scorpionate complex†

Margaux Pénicaud,[a] Edoardo Martinez,[b] Giulia Serrano,[bc] Brunetto Cortigiani,[b] Lorenzo Squillantini,[b] Juan H. González-Estefan,[a] Emilio Velez-Fort,[d] Mathieu Duttine,[a] Mathieu Gonidec,[a] Patrick Rosa,*[a] Matteo Mannini[b] and Lorenzo Poggini*[be]

Received 8th May 2023,
Accepted 24th July 2023

DOI: 10.1039/d3tc01620j

rsc.li/materials-c

A new spin-crossover complex based on a heteroscorpionate ligand was synthesized and characterized. Thin films were grown by sublimation in an ultra-high vacuum on highly oriented pyrolytic graphite (HOPG) and on single crystal Au (111), and spectroscopically characterized using X-ray absorption and X-ray photoemission. Temperature-dependent experiments on sub-nanometric deposits demonstrated that the thermally induced spin-crossover is preserved at a sub-monolayer (0.7 ML) coverage on HOPG, while films with similar thickness lose the switching behaviour when deposited on a Au(111) surface. The system was unresponsive to light stimuli at low temperatures independently of the used substrate.

1. Introduction

Spin crossover (SCO) compounds are a class of magnetic molecules[1] in which the electronic configuration of a metal ion can be changed by external stimuli.[2–5] In particular, Fe(II) based SCO complexes showing a diamagnetic and a paramagnetic state have been proposed to be employed in molecular electronic and multifunctional spintronic devices. Indeed, SCO complexes have enormous potential in this field because of the possibility to obtain active materials capable of interacting with charges (or spin) and not merely transporting them.[6–9] Furthermore, using synthetic strategies it is possible to introduce new functionalities tailoring the properties of molecular materials.[10,11] The assembly of SCO molecules on a solid support is the fundamental prerequisite for molecular-device fabrication, and high-vacuum sublimation deposition in particular is the cleanest method to obtain high-quality nanometric films suitable for this purpose, with good control of the final thickness.[12] Unfortunately, only a few SCO complexes can be heated up to their sublimation temperature without thermal degradation.[13,14] Among them are the scorpionate[15,16] complexes [FeTp$_2$] and [FeTp*$_2$] (Tp = HB(pz)$_3$, pz = 1*H*-pyrazol-1-yl, Tp* = HB(dmpz)$_3$, dmpz = 3,5-dimethyl-1*H*-pyrazol-1-yl). Both compounds show hysteretic SCO behaviour, with a conversion at high temperature for the former (300–460 K)[17] and below room temperature (240–150 K)[18,19] for the latter. Following the work of Buchen and Gütlich on this scorpionate family,[20] our goal has been focused on tuning the ligand structure to obtain a SCO complex with a room temperature conversion. Here, we report the synthesis, structural and magnetic characterization, and nanostructuration of a heteroscorpionate SCO complex [Fe(HB(pz)$_2$(dmpz))$_2$][15,20] (hereafter called **1**), the deposition of which has been attempted on highly ordered pyrolytic graphite (HOPG) and single crystal gold (Au(111)). Deposition of the complex was performed *via* ultra-high vacuum (UHV) sublimation and a full spectroscopic characterization has been performed: X-ray photoelectron spectroscopy (XPS) to confirm the integrity of the sublimated films of **1** (on HOPG and Au(111)) and X-ray absorption spectroscopy (XAS) to study the magnetic properties at the nanoscale (on both substrates). Indeed, literature reports already suggested that small changes in the structure of SCO complexes affect their switching properties[21] and a full characterization of their magnetic behaviour in nanostructures is mandatory. In nanostructured SCO complexes, the interaction with the surface can cause a total or a partial loss of the SCO properties of the system, due to a strong interaction with the substrate[22] or due to a partial degradation of the molecular structure.[23] However, the surface does not always have a negative role: an interesting modulation

[a] Univ. Bordeaux, CNRS, Bordeaux-INP, ICMCB, UMR 5026, F-33600 Pessac, Cedex, France. E-mail: patrick.rosa@icmcb.cnrs.fr
[b] Department of Chemistry "U. Schiff" (DICUS) and INSTM Research Unit, University of Florence, Via della Lastruccia 3-13, 50019 Sesto Fiorentino, FI, Italy
[c] Department of Industrial Engineering (DIEF) and INSTM Research Unit, University of Florence, Via di Santa Marta, 3, 50139, Florence, Italy
[d] European Synchrotron Radiation Facility, 71, avenue des Martyrs CS 40220, 38043 Grenoble, Cedex 9, France
[e] Institute for Chemistry of OrganoMetallic Compounds (ICCOM-CNR), Via Madonna del Piano 10, 50019 Sesto Fiorentino, Italy. E-mail: lpoggini@iccom.cnr.it

† Electronic supplementary information (ESI) available. CCDC 2261109–2261118. For ESI and crystallographic data in CIF or other electronic format see DOI: https://doi.org/10.1039/d3tc01620j

of the SCO properties, mediated by the interaction with the surface, has been observed[24] for $[Fe(H_2B(pz)_2)_2bipy]$ (bipy = 2,2′-bipyridine) deposited on dielectric surfaces such as SiO_2 and Al_2O_3. Indeed, on these surfaces, a pinning of the LS state well above the bulk transition temperature has been observed for the nanostructures of these molecules. Unlocking of the spin state, giving rise to a HS state, has been detected utilizing X-ray irradiation or mild heating as a transition stimulus. In order to avoid such surface-induced pinning effects, the use of non-metallic, weakly interacting substrates like HOPG might be a winning strategy, and indeed SCO complexes in direct contact with carbon-based substrates such as HOPG or graphene have been reported to retain switching properties.[25–29] We have thus studied the deposition of a submonolayer of **1** on Au(111) and HOPG, which are expected to promote different interactions with this molecule. We evaluated the substrate effect on the thermally induced spin crossover through the analysis of XPS and XAS spectra recorded as a function of temperature.

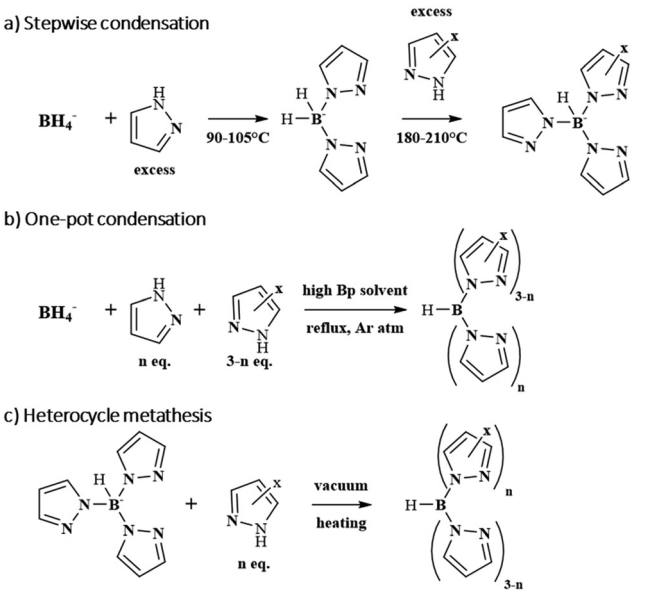

Fig. 1 Known reaction paths towards heteroscorpionate ligands. (a) Neat stepwise condensation, (b) stoichiometric condensation in solution, (c) heterocycle metathesis.

2. Results and discussion

2.1. Synthesis and properties in bulk

Complex **1** may be compared to its two homoscorpionate analogues, $[FeTp^*_2]$ and $[FeTp_2]$.[30] $[FeTp^*_2]$ is a classic example of an Fe(II) SCO complex showing HS to LS conversion upon cooling. It has regained attention since the 2010s as one of the few sublimable SCO molecules, and it was studied in bulk and thin films on various substrates. This complex has an asymmetric and hysteretic conversion[31] and shows both soft X-ray-induced spin state trapping (SOXIESST)[32–34] and remarkable light-induced spin state trapping (LIESST)[4,33,35] effects. An epitaxial relationship with Au(111) and Cu(111) was also demonstrated for submonolayers deposited on single crystals.[35,36] $[FeTp_2]$ has also attracted attention because it is sublimable and shows an LS to HS conversion above room temperature. In contrast to its methylated analogue that crystallizes in the $P\bar{1}$ space group,[19] $[FeTp_2]$ exhibits a rich polymorphism that leads to unconventional SCO behaviour.

Despite their similar structures at the molecular scale, steric hindrance and packing effects lead to very different properties of these two complexes. Hence, the idea is to modulate the properties by synthesizing a complex with intermediate composition, the heteroscorpionate **1**. The preparation of scorpionate ligands with a boron centre bearing different azole moieties is not a new idea in itself.[16] However, the very small number (<20) of publications about these specific heteroscorpionates from 1967 to date, is an indication of the difficulty of such syntheses. The first attempt, reported in 1995, is the preparation of **1** and its analogue, $[Fe(HB(pz)(dmpz)_2)_2]$, by Buchen and Gütlich.[20] Their work is based on the Trofimenko's classical procedure, a condensation of excess azole with sodium or potassium borohydride. The reaction takes place in molten azole, and the degree of substitution can be controlled by varying the reaction temperature. Thus, a stepwise condensation with different azoles had been realized (see Fig. 1a), with hardly any characterization of the obtained ligand. Wołowiec *et al.*[37] had shown later that this approach always leads to a mixture of ligands with the general formula $HB(pz)_x(pz')_{(3-x)}^-$ with x = 0–3. In the 2000s, they published a series of articles presenting different heteroscorpionate ligands[38–43] and developed a new one-pot synthesis in solution (Fig. 1b). While still leading to a mixture of ligands, this approach allowed for higher yields of the targeted heteroscorpionate. Purification was achieved after the conversion of the crude salts to their Co(II) complexes. The preparation of pure heteroscorpionate ligands was reported around the same time by Connelly *et al.*[44,45] and Desrochers *et al.*[46] Both teams adopted a similar procedure called heterocycle metathesis (Fig. 1c). The reaction proceeds by heating a homoleptic tris(pyrazolyl)borate and the other heterocycle (in their cases, triazole derivatives) under vacuum and is driven by the sublimation of the released pyrazole. This procedure was used for the quantitative substitution of pyrazole by one or two nitropyrazoles,[47] and the key parameters to control the reaction outcomes were rationalized only recently.[48]

In our case, attempts at heterocycle metathesis proved unsuccessful (see further details in the ESI†). This is likely due to the similarity between pyrazole and dimethylpyrazole, both in terms of steric hindrance and hard–soft acid–base properties (pK_a values: dmpz = 4.06, pz = 2.49, 4-nitropyrazole = −2.0).[49]

Consequently, we turned our attention to the other pathways and as expected obtained mixtures of homo- and heteroscorpionate salts from paths A and B (Fig. 1). The presence of $HB(pz)_2(dmpz)^-$ was evidenced by mass spectrometry (MS) on the crude products, with $HB(pz)_3^-$ as the main component of each mixture, and a higher fraction of the desired heteroscorpionate from path B (Fig. S2 and S3, ESI†). When using ligand B

for complexation without further purification, Fe(II) complexes could be isolated as a microcrystalline violet powder composed of aggregated tiny needles.

Elemental analysis seemed to be in reasonable agreement with the composition of complex **1**, but MS analysis revealed a mixture of complexes with the general formula $[FeH_2B_2(pz)_{6-n}(dmpz)_n]$, with n = 1–5 (Fig. S7, ESI†), the statistical distribution of which happens to present the same elemental analysis as the pure targeted complex. It is worth noting that, even though KTp predominates in the mixture of ligands, $[FeTp_2]$ is not observed in the crystals, due to higher solubility of this complex in methanol. Much improved results are obtained by simply washing the ligand mixture with diethyl ether, which significantly increases the relative amount of the target ligand to the point of making it the main component of the mix (Fig. S3, ESI†). Then, crystals of pure complex **1** can be successfully obtained by slow diffusion crystallization in methanol, as seen by MS (Fig. S6, ESI†). The product obtained is often contaminated by inorganic salts (complexation by-products) that precipitate in methanol and are easily purified by some manual triage followed by sublimation on a cold finger (5×10^{-6} mbar, 140 °C).

A single crystal of good quality was selected and allowed us to determine the structure of the complex with excellent accuracy. At 120 K, we found that the compound crystallizes in the triclinic $P\bar{1}$ space group, with two half-molecules of complex **1** in the asymmetric unit, with the iron atoms lying on special positions (see all relevant details in Table S3 (ESI†) and the inset in Fig. 2). No significant residual peaks in the Fourier electron density difference map are seen that could suggest any situational disorder of the methyl groups on the pyrazole rings, a situation that we observed in a previous crystallization batch starting from an impure ligand (see Table S3, ESI†). The structure thus confirmed that we had obtained the desired heteroscorpionate homoleptic complex. It is noteworthy that only the *trans* configuration for the two scorpionate ligands is obtained, when both *cis* and *trans* configurations are theoretically permitted, but only the *trans* configuration is compatible with the symmetry requirement induced by the special position of the iron atom at an inversion centre. The presence of two independent Fe(II) complexes in the asymmetric unit differs from the unique molecule observed for the parent compounds $[FeTp^*_2]$[19] and $[FeTp_2]$ (for what is considered to be the most stable polymorph in the monoclinic $P2_1/n$ space group).[50] Nevertheless, a similar case can be found in the first described polymorph of $[Fe(HB(pz)_3)_2]$ (in the monoclinic $P2_1/c$ space group)[51] and in the closely related [Fe(HB(3-methyl-1*H*-pyrazole)$_3$)$_2$].[52] Accordingly, the crystal packings are very different between complex **1**, $[Fe(HB(dmpz)_3)_2]$ and $[Fe(HB(pz)_3)_2]$ (Fig. S16 to S18, ESI†).

The average bond length between Fe(II) and the pyrazole ligands, at 1.984 and 1.979 Å for the two independent complexes, supports a fully low-spin (LS) state for both molecules. This is also supported by considering the distortion parameters calculated using the OCTADIST software[53] (see Table S4, ESI†) and the Continuous Symmetry[54,55] and Shape[56] Measures calculated using the online CoSym tool (see Table S5, ESI†). Indeed, the calculated values show that at 120 K, the two molecules of complex **1** are overall very close to *C*2 symmetry, with the FeN_6 coordination sphere very slightly distorted with respect to a perfect octahedron. These values are intermediate between the strongly symmetric LS structure of $[Fe(HB(dmpz)_3)_2]$ at 100 K and the slightly more distorted LS structure of $[Fe(HB(pz)_3)_2]$ at 180 K (see Tables S4 and S5, ESI†).

We collected data sets while increasing the temperature up to 380 K and then decreasing this to 300 K. Throughout these measurements, the crystalline symmetry did not change, with the triclinic $P\bar{1}$ space group (see Table S3, ESI†), and the crystal diffraction quality was preserved. The evolution of the cell volume V (Table S3 and Fig. S19, ESI†), the average Fe–N bond length, the distortion parameters Σ and Θ (Table S4 and Fig. S20, ESI†) and the Continuous Shape Measure (Table S5 and Fig. S20, ESI†) clearly support that gradual spin crossover occurs, but starting only between 250 and 300 K. The values of these parameters at 380 K were found to be intermediate between those for fully high-spin (HS) $[Fe(HB(dmpz)_3)_2]$ at rt and partially HS $[Fe(HB(pz)_3)_2]$ at 420 K, thus supporting that the spin crossover is incomplete at the highest temperature reached. Cooling down, full reversibility was observed. No difference was observed between the two independent complexes in the unit cell.

Bulk properties of the purified powder of complex **1** were assessed using ^{57}Fe Mössbauer spectroscopy at room temperature and a vibrating sample magnetometer (VSM) up to 450 K (Fig. 2). At 295 K, in agreement with the behaviour observed for single crystals, the Mössbauer spectrum shows the occurrence of two quadrupole doublets (Fig. S21, ESI†). The first is characterized by an isomer shift δ of 0.41(2) mm s^{-1} and a quadrupole splitting Δ of 0.15(5) mm s^{-1}. These values are typical for LS Fe(II), and well in line with the values obtained for LS $[FeTp_2]$ (0.41/0.22 mm s^{-1} at 295 K) and $[FeTp^*_2]$ (0.55/0.11 mm s^{-1} at 78 K).[57] The ^{57}Fe hyperfine parameters of the second doublet

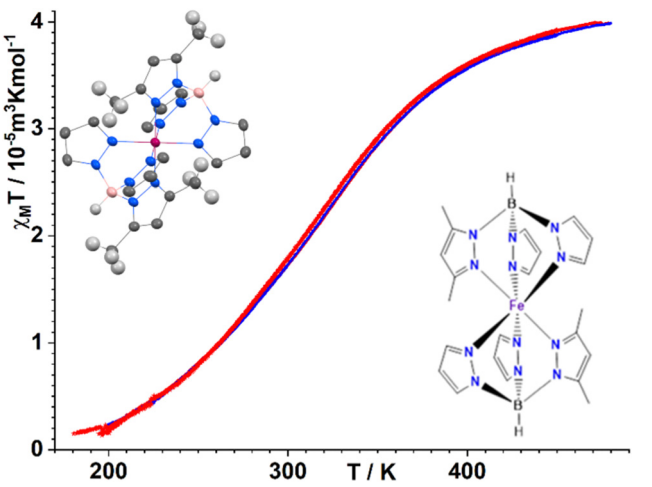

Fig. 2 Variation of the product of molar susceptibility χ with temperature for complex **1** in the 180–480 K range (two cycles are represented). Inset: Representations of the molecular structure (right) and one unit of complex **1** in the crystal structure at 120 K (left).

(δ = 1.07(4) mm s^{-1} and Δ = 3.20(9) mm s^{-1}) are characteristic of HS Fe(II) and absolutely comparable to the values obtained for HS [FeTp*$_2$] (1.03/3.67 mm s^{-1} at 300 K), or the small HS fraction surprisingly induced on [FeTp$_2$] by very high pressure (0.86/3.23 mm s^{-1} at rt under 7.8 GPa).[57] The usual approximation is to assume a similar Lamb-Mössbauer factor for the HS and LS chromophores, which leads to an HS fraction (n_{HS}) of 25 ± 5% extracted from the ratio of the resonance areas. The significantly high error in this value is mainly due to the poor signal-to-noise ratio of the collected spectrum, which is related to low values of the Lamb-Mössbauer factor at room temperature for both Fe(II) states. Moreover one can note very different linewidths for the two signals (0.53(4) and 0.82(9) mm s^{-1} respectively), which is in line with a more disordered coordination sphere for HS Fe(II) as evidenced by the crystal structures.

Magnetic susceptibility χ shows the expected behaviour for a spin-crossover complex (Fig. 2). The χT product at 180 K is 1.5 × 10^{-6} m^3 Kmol^{-1}, indicating an almost fully LS complex. It increases very gradually up to 40.6 × 10^{-6} m^3 Kmol^{-1} at 480 K, just above the 37.7 × 10^{-6} m^3 Kmol^{-1} spin-only value for a fully HS S = 2 Fe(II) complex. Considering that we have a fully HS state at this temperature, we calculated the $n_{HS}(T)$ curve and obtained a $T_{1/2}$ of 312(2) K. Fitting with a simple Boltzmann dependence[58] gives ΔH = 19.5(5) kJ mol^{-1} and ΔS = 60.8(2) JK^{-1} mol^{-1} (Fig. S22, ESI†). The latter values are in line with the usual values for SCO complexes.[58]

2.2. Characterization of thin films

As reported in the synthesis section for complex **1**, it is easy to sublimate. In order to chemically characterise sublimated deposits, a sub-monolayer on both types of surfaces has been studied by variable temperature XPS (VT-XPS) and structurally studied using STM at 25 K. It is worth noting that a low sticking coefficient has been revealed for **1** by XPS and XAS data after the first layer was deposited. Even if the initial deposition rate estimated in our apparatus was 2 nm h^{-1}, it was not possible to grow more than 1 ML, even when the surfaces were exposed for a very long time (4 hours) to the molecular flux (see Table S6, ESI†). Using STM at 25 K reveals coverage of a monolayer on both HOPG and Au(111). Using STM, it was possible to observe a molecular lattice on both surfaces (Fig. S23, ESI†), revealing the presence of an almost spherical object with a dimension of *ca.* 0.5 nm, in agreement with the average molecular dimensions taken from the crystal structure.

The stoichiometry of these deposits has been estimated by semiquantitative analysis of the XPS data and compared with the one detected for the powder sample. This elemental analysis (see Table S7, ESI†) has been performed in order to evaluate the molecular integrity of the sublimated films. For the bulk powder and for all monolayers, the N1s region features one main component at 399.9 eV (Fig. S24, ESI†) attributable to the nitrogen atoms bonded with boron and to the nitrogen atoms involved in iron coordination,[59] plus a small shake-up located at 401.4 eV. The C1s for the powder and for the monolayer on Au(111) has been fitted using three components: one related to sp^2 and sp^3 carbon at 284.4 eV (ca 42%, theoretical 45.5%), the second is given by C–N placed at 285.2 eV (58%, theoretical 54.5%) plus its shake-up placed at 286.6 eV.[60] Comprehension of the Fe2p region is a bit more difficult, due to the presence of a fine structure indicative of the valence and spin state of the iron as has been already reported by some of us for other SCO systems.[10–12] The Fe2p region has been deconvoluted with five components for both the 2p$_{1/2}$ and 2p$_{3/2}$ peaks (Fig. 3), and the peak labelled A (708.1 eV) and its satellite A' (720.7 eV) are indicative of the Fe(II) LS state. Their energy and the presence of some shake-up features are typical of a paramagnetic Fe(II) ion[61] and they have been found in both the bulk powder and the nanometric films, coherent with mixed spin states of the complex at room temperature.

The N/Fe ratio has been identified as the best parameter to evaluate molecular integrity, since iron and nitrogen signals do not overlap with other elements (*e.g.* C1s of **1** is totally covered by the contribution from HOPG crystal). The N/Fe ratio thus obtained is 12.9 for the bulk powder, 11.9 for the film on HOPG and 12.1 for Au(111), all in agreement with the theoretical value of 12.0. From this ratio, it is possible to assume that the stoichiometry of the SCO complex is retained after sublimation, both on HOPG and on Au (111). In Table S7 (ESI†), we report the complete stoichiometric analysis of the bulk and sub-monolayer coverages on HOPG and Au(111).

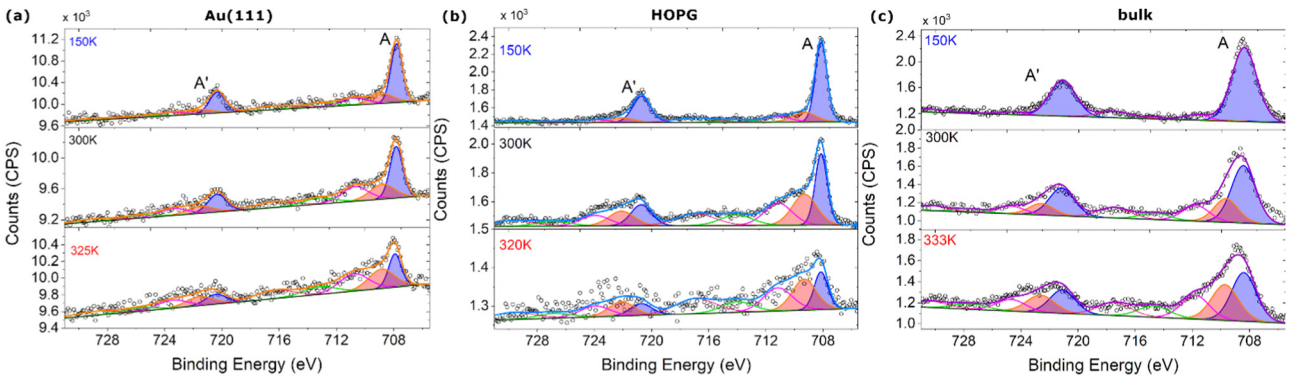

Fig. 3 (a) Thermal evolution of Fe2p XPS region spectra for 0.7 ML films on Au(111), (b) on HOPG and (c) in the bulk. Peaks linked to the LS (HS) component are highlighted in blue (red) respectively.

The spectral variations with temperature reported in Fig. 3 qualitatively reveal that spin crossover occurs for complex **1** in the bulk – as expected – but also for the sub-monolayer coverages. Nevertheless, significant deviations respective to the bulk are observed depending on the substrate. The temperature dependence of the Fe2p XPS signal on HOPG follows the trend for the SCO expected from the χT plot (Fig. 2), as seen by plotting the ratio n = (Fe2p total area minus $A + A'$ component area)/total area, which is an indication of the HS fraction as a function of the temperature (Fig. S25, ESI†). For deposition on Au(111), the temperature variation seems to be less efficient, as it is possible to see from the evolution of the ratio n *vs.* temperature shown in Fig. S25 (ESI†). Moreover, it has been observed that the reversibility after the heating procedure is not retained on Au(111), and it presents a pinning of the reversibility as is possible to observe also from Fig. S26 (ESI†), where we can see that the complex on HOPG retains a perfectly reproducible switching behaviour after every thermal cycle, while the sample on Au(111) progressively loses it. This scenario can also be followed by ultraviolet photoelectron spectroscopy (UPS),[7,10,62] that reveals an incomplete reversibility of the molecular layer once adsorbed on Au(111) in contrast to what was observed on HOPG (see Fig. S27, ESI†).

To shed some light on this behaviour, we performed a temperature-dependent XAS experiment at the ESRF ID32 beamline[63] (Fig. 4). Variable temperature spectra are related to a sub-monolayer deposition on HOPG (Fig. 4a, bottom) and on an Au(111) single crystal (Fig. 4a, top). To verify the trend obtained by XPS, the XAS spectra were acquired by cooling down starting from 320 K for both samples. For comparison, Fig. 4a shows XAS spectra at the lowest and the highest temperature for 0.7 ML of **1** on HOPG and on Au(111). To obtain a quantitative HS fraction of the two systems, experimental Fe L_3 edge spectra have been linearly interpolated employing a weighted sum of reference spectra, as described in the method section (see details in Fig. S28, ESI†). From the results of the interpolation, we have extracted the HS fraction n_{HS} for each temperature and for each sample, obtaining the plot reported in Fig. 4b. Thanks to this approach, it is possible to compare the SCO behaviour of the two nanostructured systems and the bulk material.

The line shape of the spectra recorded on the 0.7 ML nm deposit on HOPG in the range of temperature from 2 K to 320 K appears compatible with an Fe(II) system in an octahedral environment.[64] From 2 K to 200 K, complex **1** appears to be in the LS configuration, as expected from magnetometry and crystallography results on the bulk material (Fig. 2 and Fig. S20, ESI†). Increasing the temperature above 200 K, the line shape of the Fe L_3 edge evolves in line with an increase in the HS contribution, up to 320 K (maximum operating temperature of the set-up available on ID32). This is in line with our hypothesis that HOPG is an ''innocent'' surface for this compound and does not significantly influence the thermally driven spin conversion, as seen from VT-XPS spectra of other compounds on HOPG already reported by some of us[62] and others.[14,25,65–67]

On the other hand, the XAS characterization experiments carried out on a similar deposit of 0.7 ML on Au (111) (Fig. 4a), from 2 K up to 320 K, reveal a different scenario: the sample already seems to show a high contribution of the HS species even at cryogenic temperature, where only LS species should be present. As can be seen in Fig. 4(a) for **1**/Au(111), we observed the presence of other features, especially at low temperature, and this may be correlated to possible hybridization between surface states and molecular leading to a broadening and shift of the Fe edge, as reported in ref. 65, giving a lower agreement of the fits with the measured experimental data. This is a further indication of the more complex interaction of the molecule with this surface. To simplify the comparison, the high spin fraction for the bulk material is also reported in Fig. 4b, evaluated directly from the magnetic susceptibility data.[68] This comparison shows that the magnetic behaviour of molecules of **1** on HOPG is comparable with the bulk, even in the case of 0.7 ML, where the investigated molecules are in direct contact with the surface. As mentioned above, the spectra of complex **1** on Au(111) show the coexistence of HS and LS

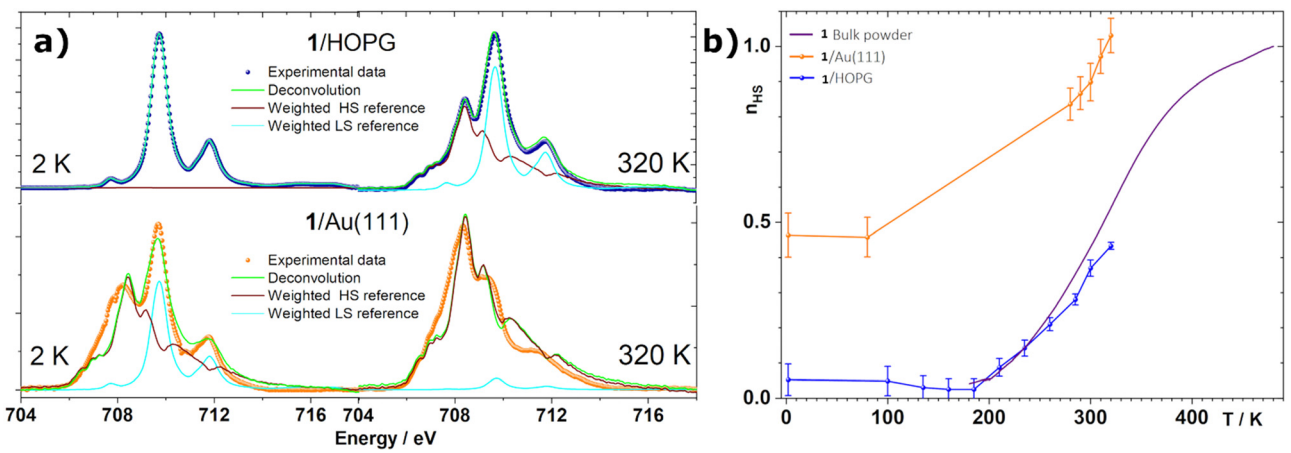

Fig. 4 (a) Thermal evolution of XAS spectra at the Fe L_3 edge for 0.7 ML films on HOPG (top) and Au(111) (bottom); (b) variation of nHS (obtained from the linear regression) as a function of temperature.

states even at cryogenic temperature, suggesting a modification of the coordination environment with respect to intact molecules induced by the gold surface. On the other hand, the spectra show a small evolution upon increasing the temperature and this may be attributed to the presence of a fraction of intact molecules preserving the SCO behaviour. These effects could be ascribed also to hybridization with surface states, leading to a broadening and chemical shift of the Fe edge.[65] It is noteworthy that similar spin pinning effects are reported in the literature for sub-monolayers and thin films of $[Fe(Tp^*)_2]$ on Au(111)[33,36,69] and Cu(111).[70,71]

A relevant parameter that can be extracted from the XAS spectra is the branching ratio, defined as the ratio between the integrated intensity of the L_3 iron edge and the total edges ($L_3 + L_2$). The dependence of this ratio with temperature can be used to evaluate the spin transition. The obtained branching ratio values at 2 K and 320 K are, respectively, 0.63 and 0.74 for the 0.7 ML film on HOPG, and 0.75 and 0.72 for the sub-monolayer on Au(111). The two values for HOPG are in line with the values reported in the literature for another SCO complex[72] (0.77 and 0.67 at room temperature and 6 K respectively). The gradual decrease in the branching ratio from high to low temperatures is typical for HS–LS crossover, due to the vanishing of the spin-orbit coupling in the initial state. Under these conditions, the hole has randomly oriented spin and angular momenta and the integrated intensities of L_3 and L_2 iron edges depend exclusively on the final state statistics.[73,74] Indeed, the branching ratio values are in good agreement also with calculated values, obtained elsewhere evaluating both the statistical term (all the possible final states $2p^n3d^m$–$2p^{n-1}3d^{m+1}$) and the spin–orbit coupling between the core hole and final state. The calculated values are 0.66 for a 100% LS state and 0.79 for a 100% HS state.[75] On the other hand, the branching ratio of complex **1** on Au(111) changes very little, indicating a small fraction of the SCO behaviour. The L_3 main features positions (together with branching ratio values) are reported in the ESI† (Table S8).

Recent works report that the Soft X-ray Induced Electron Spin State Trapping (SOXIESST)[32–34] effect can be activated by the interaction with SCO molecules and the surface.[14,67,76,77] In the present case, at cryogenic temperatures, SOXIESST cannot be observed in either sub-monolayer sample. Accordingly, even under green (516 nm) and red (660 nm) light irradiation, no Light-Induced Spin State Trapping (LIESST)[78] has been detected in the 0.7 ML film on HOPG (see Fig. S29 in the ESI†). We checked by performing a photomagnetic experiment on bulk microcrystalline powder in a SQUID magnetometer equipped with a dedicated setup.[79,80] Some very limited photoconversion (a few %, see Fig. S30 in ESI†) was observed using either 532 or 650 nm laser light, but the relaxation was observed to be quite fast, with a T(LIESST) of around 14 K. No significant reverse-LIESST effect was observed when irradiating at 830 nm. This quite fast relaxation of the photoinduced state could be expected on the basis of the relatively high SCO $T_{1/2}$ of 312 K, while the limited photoconversion is certainly due to the strong purple colour of the complex in the LS state. While absorption effects are absent for the submonolayer deposits, the total absence of photoinduced effect may point to the surface inducing an even faster relaxation, making it so that the metastable photoexcited state has a shorter lifetime than the XAS measurement.

3. Conclusions

Although SCO complexes have been studied in an enormous variety of nanostructures, only a few examples of molecules sublimable under high vacuum and retaining their switching behaviour at the monolayer level have been reported so far. In light of the very interesting properties shown by [Fe(Tp*)2], with remarkable SOXIESST,[32–34] LIESST[4,33,35] properties and epitaxial growth on Au(111) and Cu(111) single crystals,[35,36] we engineered the synthesis of a mixed heteroscorpionate ligand which yielded complex **1**. Complex **1** showed gradual spin crossover above room temperature. Its isolation as a pure species allowed us to show that it can be thermally sublimated in a high-vacuum environment into monolayer films.

In this study, we demonstrated that the SCO complex **1** can be deposited on a surface while conserving its chemical integrity, that the thermally induced SCO is retained and does not change significantly, at the monolayer level, when compared to the reference crystalline bulk sample once the SCO has been sublimated on HOPG.

This study confirms that HOPG surfaces are weakly interacting substrates suitable for the deposition of SCO molecules. On the other hand, Au(111) surfaces modify the SCO behaviour of the same compound. Therefore, the crucial role played by the interface between molecular SCO materials and inorganic materials has been confirmed. This understanding paves the way towards molecular hybrid, multifunctional electronic and spintronic devices based on SCO complexes. Thanks to the temperature range of the investigated SCO enclosing room temperature, experiments aimed at investigating the electrical conductance of nanometric films of complex **1** are currently underway in our laboratories.

4. Methods

Synthesis of $KHB(pz)_2(dmpz)$

The procedure was adapted from ref. 42. In a 250 mL round-bottom flask, 1069 mg (19.8 mmol) of KBH_4, 2722 mg (40 mmol) of pyrazole and 1924 mg (20 mmol) of 3,5-dimethylpyrazole are suspended in 60 mL of hexadecane. The flask is equipped with a Vigreux column connected to an argon line and a volume meter. The experimental setup is purged under a flow of argon for 30 min prior to the reaction. The reaction mixture is heated from room temperature to 278 °C over the course of 4 hours, with constant stirring. At this point, the theoretical amount of hydrogen (1.47 L, 60 mmol) had evolved from the reaction. Heating was continued for 30 minutes, then the reaction mixture was allowed to cool down to 100 °C. 100 mL of heptane was added and the mixture was left to stand at rt overnight.

Upon cooling, the product formed a compact white mass at the bottom of the reaction flask and was impossible to recover. The solvents were then removed, and the solid was rinsed with 3 × 20 mL of heptane. 60 mL of toluene was poured onto the solid and the product was left to dissolve for 4 days. The resulting suspension was filtered and the toluene was removed under reduced pressure. The crude product was obtained as a white viscous solid. It was then suspended in 81 mL of Et_2O and filtered to obtain a white powder. Mass spectrometry showed that the product was a mixture containing both $KHB(pz)_2(dmpz)$ as the main product, and $KHB(pz)_3$ as a side product.

Synthesis of $[Fe(HB(pz)_2(dmpz))_2]$

The Fe(II) complex was prepared by slow diffusion crystallization in freshly distilled methanol. In two separated Schlenk tubes, 90.8 mg (0.325 mmol) of $FeSO_4{\cdot}7H_2O$ and 192.9 mg (0.65 mmol) of the ligand $KHB(pz)_2(dmpz)$ were weighed. The starting materials were placed under an argon atmosphere and dissolved in 3 mL of methanol. A separation layer (4 mL of pure methanol) was slowly added on top of the iron solution, and then the ligand solution was slowly added on top of the separation layer. The solutions were allowed to diffuse for five days, after which the solution was removed and the product dried under reduced pressure. In order to separate the compound from the potassium salts precipitated during diffusion, the reaction products were suspended in ethanol and filtered, and then washed with small amounts of water until the liquid phase remained colourless. It was then rinsed with ethanol and dried in air. The complex was obtained as dark violet microcrystals (37.6 mg, 21% yield).

Powder X-ray diffraction

Powder X-ray diffraction patterns were recorded on a PANalytical X'Pert MPD PRO diffractometer with Bragg–Brentano geometry, Cu Kα radiation (λ = 1.54184 Å) and a secondary graphite 370 monochromator. It was measured on an aluminium sample holder, in the 8–80° 2θ angular range over 2096s. Data were analyzed using the Jana2006 software.[81]

Single-crystal X-ray diffraction

Single-crystal X-ray diffraction experiments were performed on a Bruker-Nonius κ-CCD diffractometer with Mo Kα radiation (0.71073 Å). Data collection was performed between 120 and 380 K, using an Oxford CryoSystem 700 installed on the diffractometer, with the crystal glued to a glass fiber using nail varnish. Data were collected using sets of ω scans at different ϕ or 2θ angles, reduced and scaled using the DENZO and Scalepack softwares.[82] The structural determination by intrinsic phasing and the refinement of atomic parameters based on full-matrix least squares on F^2 were performed using the SHELXT[83] and SHELXL-2018[84] programs within the Olex2 package.[85] All refinement details are given in Table S3 in the ESI.† Hydrogen atoms were identified by their respective electron density peaks in Fourier difference maps, then refined isotropically using riding constraints.

Magnetic measurements

Magnetic measurements were performed on a Microsense EZ-7 Vibrating Sample magnetometer. Samples were accurately weighed using a Mettler MX5 microbalance, and then enclosed in Säntis light tin capsules for solids. The diamagnetic contributions of the sample holders were determined separately and were subtracted accordingly from the measurements, which were further corrected for the sample diamagnetism using Pascal constants.[86] Photomagnetic measurements were performed on a Quantum Design MPMS-7XL SQUID magnetometer. The bulk sample was weighed by difference using a Mettler-Toledo MX5 microbalance. 0.505 mg of sample was fixed on double-faced scotch tape, using some plastic film and a straw cut in half as support. Irradiation was performed using a homemade sample rod with an NA0.22 optical fiber. A fibered optical bench with laser diodes provided 405, 532, 650, 830 and 980 nm irradiation. No effect was observed at 405, 830 and 980 nm, photoconversion was very slow at 650 nm. Fluence at 532 nm was 18 mW cm^{-2} on the sample.

Mössbauer spectroscopy

A few milligrams of sample were encapsulated in Mylar and ^{57}Fe transmission Mössbauer spectra were recorded in transmission geometry using a constant acceleration Halder–type spectrometer with a room temperature ^{57}Co source (embedded in Rh matrix). The velocity scale was calibrated according to the ^{57}Fe Mössbauer spectrum of a pure α-Fe(0) foil recorded at room temperature. The Mössbauer hyperfine parameters (δ isomer shift, Δ quadrupole splitting, Γ Lorentzian linewidth and relative areas) were refined using both homemade programs and the WinNormos® software (Wissenschaftliche Elektronik GmbH).

Vacuum sublimation

Vacuum sublimation was carried out using a home-made Knudsen cell, the sublimation temperature was 410 K measured with a K thermocouple with a base pressure of 10^{-8} mbar. The same Knudsen cell was employed to sublimate *in situ* with a base pressure of $10^{-9}/10^{-10}$ mbar at ID32 beamline at ESRF.[63] For in-house experiments and for large scale experiments, the nominal thickness was estimated using a quartz crystal microbalance (QCM).

XPS

XPS data were acquired using monochromatic Al Kα radiation ($h\nu$ = 1486.6 eV, SPECS mod. XR-MS focus 600) operating at a power of 100 W (13 kV and 7.7 mA) and a SPECS Phoibos 150 1-DLD electron analyser mounted at 54.4° respect to the X-ray source. The XPS spectra were recorded for normal emission with the fixed pass energy set to 40 eV. The spectra were analysed using the CasaXPS software. All the spectra were calibrated to the Fermi value of the substrate. The background in the spectra was subtracted using a linear background, and the deconvolution of the XPS spectra was carried out as a combination of Gaussian and Lorentzian functions (70/30).

Calculated cross-sections[87] have been used instead of semi-empirical sensitivity factors for semiquantitative analysis. XPS spectra related to N1s, C1s, B1s and Fe2p have been deconvoluted employing the same Voigt components for both bulk powders and deposited films. The variable temperature experiment was performed by using a liquid nitrogen-based cryostat connected to the XPS sample holder. Every spectrum represented herein results from the averaging of 16 spectra collected after 1 h of thermalisation at a specific temperature.

STM

STM measurements were carried out using an Omicron VT-STM at 25 K for the characterization of molecular deposits. All the images were acquired using an electrochemically etched W tip. Images were analysed with the Gwyddion software.[88]

HOPG (ZYA grade, purchased from NT-MDT) was freshly exfoliated and once introduced in UHV warmed up to 420 K immediately before the deposition that was then performed when this substrate was back at room temperature. The Au(111) single crystal was freshly prepared using a standard procedure involving sputtering and annealing.

XAS

XAS characterization was performed at ID32 at the European Synchrotron Radiation Facility (ESRF) on a UHV compatible pumped ^{4}He cryo-magnet.[63] XAS spectra were measured in total electron yield (TEY) detection mode to guarantee the optimal surface detection sensitivity, from 2 K up to 320 K (maximum reachable temperature). All the characterization experiments were performed using a low density of photons in order to avoid radiation damage, which was verified by the absence of evolution of rt spectra. Estimation of the temperature dependence of the n_{HS}–Fe(II) molar fraction of the submonolayer coverage was performed through least-squares interpolation of normalized L_3 XAS spectra with two reference spectra of 100% LS and 100% HS, as we have already done previously.[62,64,89] These reference spectra have been obtained from experimental data acquired during this experiment: 100% LS reference is the spectrum related to 0.7 ML film on HOPG measured at 2 K, while 100% HS reference has been obtained from the spectrum measured at 320 K, with the hypothesis that it is the sum of the HS and LS components and thus subtracting as much LS reference as possible while keeping the resulting spectrum positive. Irradiation experiments were performed using a ThorLabs CLD101 compact laser diode controller, and 516 and 660 nm single mode fiber-pigtailed laser diodes. Laser light was directed inside the UHV cryo-magnetic chamber through a glass view port using a fibered reflective collimator, at a distance of *ca.* 36 cm of the sample, with a laser spot about 1 cm width and fluences on the same order of magnitude than our photomagnetic experiments.

Conflicts of interest

There are no conflicts to declare.

Acknowledgements

LS acknowledges the support of European COST MOLSPIN (CA15128) for funding his stay in Bordeaux. JHGE acknowledges the support of the Mexican government *via* the National Council of Sciences and Technology (CONACyT, program 073096, announcement 291060).We acknowledge the financial support from: the French National Research Agency (ANR) Investment for the Future Programme IdEx Bordeaux (ANR-10-IDEX-03-02), from the Université de Bordeaux, Région Nouvelle-Aquitaine, as well as from the Italian Ministry of University and Research throuh the National Recovery and Resilience Plan (NRRP, Mission 4 Component 2 Investment 1.3 - Call for tender No. 341 of 15/03/2022 funded by the European Union – NextGenerationEU, award number PE0000023, Concession Decree No. 1564 of 11/10/2022 (CUP D93C22000940001) Project title "National Quantum Institute", and through the project "Dipartimenti di Eccellenza 2023-2027, DICUS 2.0" (CUP B97G22000740001) attributed to the Department of Chemistry "Ugo Schiff" of the University of Florence. Authors gratefully acknowledge proofing by Rebecca Rodrigues de Miranda and the ESRF ID-32 staff for the experimental support (CH 5180).

References

1 P. Gütlich, *et al.*, Spin State Switching in Iron Coordination Compounds, *Beilstein J. Org. Chem.*, 2013, **9**, 342, DOI: 10.3762/bjoc.9.39.
2 S. Brooker, Spin Crossover with Thermal Hysteresis: Practicalities and Lessons Learnt, *Chem. Soc. Rev.*, 2015, **44**, 2880, DOI: 10.1039/C4CS00376D.
3 John J. McGravey and Ian Lawthers, Photochemically-Induced Perturbation of the 1A ⇌ 5T Equilibrium in Fe11 Complexes by Pulsed Laser Irradiation in the Metal-to-Ligand Charge-Transfer Absorption Band, *J. Chem. Soc., Chem. Commun.*, 1982, 906, DOI: 10.1039/C39820000906.
4 S. Decurtins, *et al.*, Light-Induced Excited Spin State Trapping in a Transition-Metal Complex: The Hexa-1-Propyltetrazole-Iron (II) Tetrafluoroborate Spin-Crossover System, *Chem. Phys. Lett.*, 1984, **105**, 1, DOI: 10.1016/0009-2614(84)80403-0.
5 P. Gütlich, *et al.*, Pressure Effect Studies on Spin Crossover Systems, *Coord. Chem. Rev.*, 2005, **249**, 1811, DOI: 10.1016/j.ccr.2005.01.022.
6 C. Lefter, *et al.*, Current Switching Coupled to Molecular Spin-States in Large-Area Junctions, *Adv. Mater.*, 2016, 7508, DOI: 10.1002/adma.201601420.
7 L. Poggini, *et al.*, Vertical Tunnel Junction Embedding a Spin Crossover Molecular Film, *Adv. Electron. Mater.*, 2018, 1800204, DOI: 10.1002/aelm.201800204.
8 G. Molnár, *et al.*, Spin Crossover Nanomaterials: From Fundamental Concepts to Devices", *Adv. Mater.*, 2018, **30**, 1703862, DOI: 10.1002/adma.201703862.
9 L. Poggini, *et al.*, Temperature-Induced Transport Changes in Molecular Junctions Based on a Spin Crossover Complex, *J. Mater. Chem. C*, 2019, **7**, 5343, DOI: 10.1039/c8tc06587j.

10 L. Poggini, *et al.*, Room Temperature Control of Spin States in a Thin Film of a Photochromic Iron(II) Complex, *Mater. Horiz.*, 2018, **5**, 506, DOI: 10.1039/C7MH01042G.
11 H. Nishikawa, H. Oshio, M. Nihei and N. Takahashi, Spin-Crossover Behavior and Electrical Conduction Property in Iron(II) Complexes with Tetrathiafulvalene Moieties, *Dalton Trans.*, 2011, **40**, 2154.
12 M. Atzori, *et al.*, Thermal and Light-Induced Spin Transition in a Nanometric Film of a New High-Vacuum Processable Spin Crossover Complex, *J. Mater. Chem. C*, 2018, **6**, 8885, DOI: 10.1039/C8TC02685H.
13 K. S. Kumar, *et al.*, Sublimable Spin-Crossover Complexes: From Spin-State Switching to Molecular Devices, *Angew. Chem., Int. Ed.*, 2021, **60**, 7502, DOI: 10.1002/anie.201911256.
14 L. Kipgen, *et al.*, Spin-Crossover Molecules on Surfaces: From Isolated Molecules to Ultrathin Films, *Adv. Mater.*, 2021, **33**, 2008141, DOI: 10.1002/ADMA.202008141.
15 S. Trofimenko, *Scorpionates: The Coordination Chemistry Of Polypyrazolylborate Ligands*, London, 1999.
16 S. Trofimenko, Recent Advances in Poly(Pyrazolyl)Borate (Scorpionate) Chemistry, *Chem. Rev.*, 1993, **93**, 943, DOI: 10.1021/cr00019a006.
17 F. Grandjean, *et al.*, Study of the High-Temperature Spin-State Crossover in the Iron(II) Pyrazolylborate Complex Fe[HB(Pz)3]2, *Inorg. Chem.*, 1989, **28**, 4406, DOI: 10.1021/ic00323a024.
18 J. P. Jesson, *et al.*, Mössbauer and Magnetic Susceptibility Investigation of the 5T2-1A1 Crossover in Some Octahedral Ferrous Complexes in the Solid State, *J. Chem. Phys.*, 1968, **48**, 2058, DOI: 10.1063/1.1669016.
19 O. Iasco, *et al.*, The Disentangling of Hysteretic Spin Transition, Polymorphism and Metastability in Bistable Thin Films Formed by Sublimation of Bis(Scorpionate) Fe(II) Molecules, *J. Mater. Chem. C*, 2017, **5**, 11067, DOI: 10.1039/C7TC03276E.
20 P. G. T. Buchen, Substituent Effects on the Spin Equilibrium in Iron(II) Pyrazolylborate Complexes, *Inorg. Chim. Acta*, 1995, **231**, 221.
21 M. A. Halcrow, Structure: Function Relationships in Molecular Spin-Crossover Complexes W, *Chem. Soc. Rev.*, 2011, 4119, DOI: 10.1039/c1cs15046d.
22 T. Miyamachi, *et al.*, Robust Spin Crossover and Memristance across a Single Molecule, *Nat. Commun.*, 2012, **3**, 936, DOI: 10.1038/ncomms1940.
23 T. G. Gopakumar, *et al.*, Spin-Crossover Complex on Au(111): Structural and Electronic Differences between Mono- and Multilayers, *Chem. – A Eur. J.*, 2013, **19**, 15702, DOI: 10.1002/chem.201302241.
24 X. Zhang, *et al.*, Locking and Unlocking the Molecular Spin Crossover Transition, *Adv. Mater.*, 2017, **29**, 1, DOI: 10.1002/adma.201702257.
25 M. Bernien, *et al.*, Spin Crossover in a Vacuum-Deposited Submonolayer of a Molecular Iron(II) Complex'', *J. Phys. Chem. Lett.*, 2012, **3**, 3431, DOI: 10.1021/jz3011805.
26 N. Konstantinov, *et al.*, Electrical Read-out of Light-Induced Spin Transition in Thin Film Spin Crossover/Graphene Heterostructures, *J. Mater. Chem. C*, 2021, **9**, 2712, DOI: 10.1039/d0tc05202g.
27 S. K. Karuppannan, *et al.*, Room Temperature Conductance Switching in a Molecular Iron(III) Spin Crossover Junction, *Chem. Sci.*, 2021, **12**, 2381, DOI: 10.1039/D0SC04555A.
28 M. Gavara-Edo, *et al.*, Sublimable Complexes with Spin Switching: Chemical Design, Processing as Thin Films and Integration in Graphene-Based Devices, *J. Mater. Chem. C*, 2023, **11**, 8107, DOI: 10.1039/D2TC04120K.
29 M. Gavara-Edo, *et al.*, Electrical Sensing of the Thermal and Light-Induced Spin Transition in Robust Contactless Spin-Crossover/Graphene Hybrid Devices, *Adv. Mater.*, 2022, 34, DOI: 10.1002/adma.202202551.
30 G. J. Long, *et al.*, Spin Crossover in Pyrazolylborate and Pyrazolylmethane Complexes, *Top. Curr. Chem.*, 2004, **233**, 91, DOI: 10.1007/b13530.
31 V. Davesne, *et al.*, Hysteresis and Change of Transition Temperature in Thin Films of Fe{[Me2Pyrz]3BH}2, a New Sublimable Spin-Crossover Molecule, *J. Chem. Phys.*, 2015, **142**, 194702, DOI: 10.1063/1.4921309.
32 V. Davesne, *et al.*, First Glimpse of the Soft X-Ray Induced Excited Spin-State Trapping Effect Dynamics on Spin Crossover Molecules, *J. Chem. Phys.*, 2013, 139, DOI: 10.1063/1.4818603.
33 K. Bairagi, *et al.*, Temperature-, Light-, and Soft X-Ray-Induced Spin Crossover in a Single Layer of Fe II -Pyrazolylborate Molecules in Direct Contact with Gold, *J. Phys. Chem. C*, 2018, **122**, 727, DOI: 10.1021/acs.jpcc.7b11874.
34 D. Collison, *et al.*, Soft X-Ray Induced Excited Spin State Trapping and Soft X-Ray Photochemistry at the Iron L2,3 Edge in [Fe(Phen)2(NCS)2] and [Fe(Phen)2(NCSe)2] (Phen = 1,10-Phenanthroline), *J. Chem. Soc. Dalton Trans.*, 1997, 4371, DOI: 10.1039/a703728g.
35 L. Zhang, *et al.*, Anomalous Light-Induced Spin-State Switching for Iron(II) Spin-Crossover Molecules in Direct Contact with Metal Surfaces, *Angew. Chem., Int. Ed.*, 2020, **59**, 13341, DOI: 10.1002/anie.202003896.
36 C. Fourmental, *et al.*, Importance of Epitaxial Strain at a Spin-Crossover Molecule–Metal Interface'', *J. Phys. Chem. Lett.*, 2019, **10**, 4103, DOI: 10.1021/acs.jpclett.9b01303.
37 T. Ruman, *et al.*, ''Complexes of Heteroscorpionate Trispyrazolylborate Anionic Ligands. Part V. X-Ray Crystallographic Studies of Cobalt(II) Complexes with Hydrobis(3,5-Dimethylpyrazolyl)(3,5-Diphenylpyrazolyl)Borate and Hydrobis(3,5-Diphenylpyrazolyl)(3,5-Dimethylpyrazolyl)'', *Polyhedron*, 2001, **20**, 2965, DOI: 10.1016/S0277-5387(01)00911-1.
38 M. Lukasiewicz, *et al.*, Complexes of Heteroscorpionate Trispyrazolylborate Anionic Ligands Part I. The Crystal Structure and Reactivity of Thiocyanato[Hydrobis(3-Phenylpyrazolyl)(3-Tert-Butylpyrazolyl)-Borato]Cobalt(II) Complex, *Polyhedron*, 2000, **19**, 2119, DOI: 10.1016/S0277-5387(00)00512-X.
39 T. Ruman, *et al.*, ''Complexes of Heteroscorpionate Trispyrazolylborate Anionic Ligands. Part III. X-Ray Crystallographic and NMR1 Studies on Cobalt(II) Complexes with

Tris(Pyrazolyl)Borate Anionic Ligands Obtained from 3,5-Di-Methylpyrazole and 3(5)-Methyl,5(3)-Phenylpyrazol'', *Polyhedron*, 2001, **20**, 2551, DOI: 10.1016/S0277-5387(01)00854-3.

40 T. Ruman, *et al.*, Anionic Poly(Pyrazolyl)Borate Ligands Obtained from 3,5-Dimethylpyrazole and 3,5-Diphenylpyrazole and Their Cobalt(II) Complexes – X-Ray Crystallographic And1H NMR Studies, *Eur. J. Inorg. Chem.*, 2002, 754.

41 T. Ruman, *et al.*, The Ambivalent Bonding of the 3(5)-Isopropylpyrazolyl Moiety in Homo- and Heteroscorpionate Hydrobis(3-R1-5-R2-Pyrazolyl)(y-Isopropylpyrazolyl)- Boratocobalt(II) Complexes (y = 3 or 5), *Eur. J. Inorg. Chem.*, 2003, 89, DOI: 10.1002/ejic.200390017.

42 T. Ruman, *et al.*, Complexes of Heteroscorpionate Trispyrazolylborate Ligands. Part IX. X-Ray Crystallographic Studies on Cobalt(II) Complexes of Hydrobis(3-Phenyl,5-Methylpyrazolyl)(3,5-Diethylpyrazolyl)Borate, *Polyhedron*, 2003, **22**, 581, DOI: 10.1016/S0277-5387(03)00002-0.

43 T. Ruman, *et al.*, Complexes of Heteroscorpionate Trispyrazolylborate Ligands. Part 10. Structures and Fluxional Behavior of Rhodium(I) Complexes with Heteroscorpionate Trispyrazolylborate Ligands, Tp″Rh(LL) (LL = (CO)2 or COD, *Organometallics*, 2003, **22**, 1072, DOI: 10.1021/om020873x.

44 R. J. Blagg, *et al.*, Isomerism in Rhodium(I) N,S-Donor Heteroscorpionates: Ring Substituent and Ancillary Ligand Effects, *Dalton Trans.*, 2010, **39**, 11616, DOI: 10.1039/c0dt00774a.

45 M. J. López-Gómez, *et al.*, Potassium S2N-Heteroscorpionates: Structure and Iridaboratrane Formation, *Dalton Trans.*, 2011, **40**, 4647, DOI: 10.1039/c0dt01718c.

46 P. J. Desrochers, *et al.*, Immobilized Boron-Centered Heteroscorpionates: Heterocycle Metathesis and Coordination Chemistry, *Inorg. Chem.*, 2011, **50**, 1931, DOI: 10.1021/ic102392x.

47 H. Flötotto, *et al.*, Amine-Functionalized Spin Crossover Building Blocks, *Eur. J. Inorg. Chem.*, 2019, 4621, DOI: 10.1002/ejic.201900916.

48 C. Ma, *et al.*, Precise Control of the Degree and Regioselectivity of Functionalization in Nitro- And Amino-Functionalized Di(Trispyrazolylborato)Iron(Ii) Spin Crossover Complexes, *Dalton Trans.*, 2021, **50**, 18077, DOI: 10.1039/d1dt03445f.

49 V. Lopez, *et al.*, On the Relationship between Thermodynamic p K a's of Azoles and the Oxidation Potentials of Their Pentacyanoferrate(II) Complexes, *Can. J. Chem.*, 1990, **68**, 958, DOI: 10.1139/v90-149.

50 L. Salmon, *et al.*, Re-Investigation of the Spin Crossover Phenomenon in the Ferrous Complex [Fe(HB(Pz)3)2], *New J. Chem.*, 2009, **33**, 1283, DOI: 10.1039/b902811k.

51 J. D. Oliver, *et al.*, Iron-Nitrogen Bond Lengths in Low-Spin and High-Spin Iron(II) Complexes with Poly(Pyrazolyl)Borate Ligands'', *Inorg. Chem.*, 1980, **19**, 165, DOI: 10.1021/ic50203a034.

52 S. Calogero, *et al.*, ''A Mössbauer Study of Some Iron(II) and Iron(III) Poly(Pyrazolyl)Borates. The x-Ray Crystal Structures of Iron(II)Bis[Hydridotris(3-Methyl-1H-Pyrazol-1-Yl)Borate] and Iron(II)Bis[Hydridotris(1H-Pyrazol-1-Yl)Borate] Tetrafluoroborate'', *Polyhedron*, 1994, **13**, 87, DOI: 10.1016/S0277-5387(00)86642-5.

53 R. Ketkaew, *et al.*, OctaDist: A Tool for Calculating Distortion Parameters in Spin Crossover and Coordination Complexes, *Dalton Trans.*, 2021, **50**, 1086, DOI: 10.1039/D0DT03988H.

54 M. Pinsky, *et al.*, Analytical Methods for Calculating Continuous Symmetry Measures and the Chirality Measure, *J. Comput. Chem.*, 2008, **29**, 2712, DOI: 10.1002/jcc.20990.

55 G. Alon, *et al.*, Improved Algorithms for Symmetry Analysis: Structure Preserving Permutations, *J. Math. Chem.*, 2018, **56**, 193, DOI: 10.1007/s10910-017-0788-y.

56 S. Alvarez, Distortion Pathways of Transition Metal Coordination Polyhedra Induced by Chelating Topology, *Chem. Rev.*, 2015, **115**, 13447, DOI: 10.1021/acs.chemrev.5b00537.

57 G. J. Long, *et al.*, Spin Equilibrium in Iron(II) Poly(1-Pyrazolyl)Borate Complexes: Low-Temperature and High-Pressure Mössbauer Spectral Studies, *Inorg. Chem.*, 1987, **26**, 608, DOI: 10.1021/ic00251a023.

58 W. Nicolazzi, *et al.*, Thermodynamical Aspects of the Spin Crossover Phenomenon, *C. R. Chim.*, 2018, **21**, 1060, DOI: 10.1016/j.crci.2018.10.003.

59 M. P. Gil, J. H. dos Santos and O. L. Casagrande Jr, Copolymerization of Ethylene with 1-Hexene Using Sterically Hindered Tris(Pyrazolyl)Borate Titanium (IV) Compounds, *Macromol. Chem. Phys.*, 2001, **202**, 319.

60 M. Pellei, *et al.*, Synthesis and Properties of Poly(Pyrazolyl)-Borate and Related Boron-Centered Scorpionate Ligands. Part B: Imidazole-, Triazole- and Other Heterocycle-Based Systems, *Mini. Rev. Org. Chem.*, 2010, **7**, 173, DOI: 10.2174/157019310791384146.

61 I. A. L. Yin, Paramagnetism and Shake-up Satellites in X-Ray Photoelectron Spectra, *Chem. Phys. Lett.*, 1973, 24.

62 L. Poggini, *et al.*, Surface Effects on a Photochromic Spin-Crossover Iron(II) Molecular Switch Adsorbed on Highly Oriented Pyrolytic Graphite, *Nanoscale*, 2019, **11**, 20006, DOI: 10.1039/C9NR05947D.

63 K. Kummer, A. Fondacaro, E. Jimenez, E. Velez-Fort, A. Amorese, M. Aspbury, F. Yakhou-Harris, P. Van Der Linden and N. B. Brookes, The High-Field Magnet Endstation for X-Ray Magnetic Dichroism Experiments at ESRF Soft X-Ray Beamline ID32, *J. Synchrotron Radiat.*, 2016, **23**, 464, DOI: 10.1107/S160057751600179X.

64 B. Warner, *et al.*, Temperature- and Light-Induced Spin Crossover Observed by X-Ray Spectroscopy on Isolated Fe(II) Complexes on Gold, *J. Phys. Chem. Lett.*, 2013, **4**, 1546, DOI: 10.1021/jz4005619.

65 K. Diller, *et al.*, Interpretation of X-Ray Absorption Spectroscopy in the Presence of Surface Hybridization, *J. Chem. Phys.*, 2017, **146**, 214701, DOI: 10.1063/1.4984072.

66 S. Ossinger, *et al.*, Effect of Ligand Methylation on the Spin-Switching Properties of Surface-Supported Spin-Crossover Molecules, *J. Phys.: Condens. Matter*, 2019, **32**, 114003, DOI: 10.1088/1361-648X/AB5C92.

67 S. Thakur, *et al.*, Thermal- And Light-Induced Spin-Crossover Characteristics of a Functional Iron(II) Complex at Submonolayer Coverage on HOPG, *J. Phys. Chem. C*, 2021, **125**, 13925.

68 P. Gütlich, *et al.*, Spin Crossover Phenomena in Fe(II) Complexes, *Chem. Soc. Rev.*, 2000, **29**, 419, DOI: **10.1039/b003504l**.
69 K. Bairagi, *et al.*, Molecular-Scale Dynamics of Light-Induced Spin Cross-over in a Two-Dimensional Layer, *Nat. Commun.*, 2016, **7**, 1, DOI: **10.1038/ncomms12212**.
70 M. Kelai, *et al.*, Thermal Bistability of an Ultrathin Film of Iron(II) Spin-Crossover Molecules Directly Adsorbed on a Metal Surface, *J. Phys. Chem. Lett.*, 2021, **12**, 6152, DOI: **10.1021/acs.jpclett.1c01366**.
71 Y. Tong, *et al.*, Voltage-Induced Bistability of Single Spin-Crossover Molecules in a Two-Dimensional Monolayer, *J. Phys. Chem. Lett.*, 2021, **12**, 11029, DOI: **10.1021/acs.jpclett.1c03271**.
72 M. Bernien, *et al.*, Highly Efficient Thermal and Light-Induced Spin-State Switching of an Fe(II) Complex in Direct Contact with a Solid Surface, *ACS Nano*, 2015, **9**, 8960, DOI: **10.1021/acsnano.5b02840**.
73 B. T. Thole, *et al.*, Branching Ratio in X-Ray Absorption Spectroscopy, *Phys. Rev. B: Condens. Matter Mater. Phys.*, 1988, **38**, 3158, DOI: **10.1103/PhysRevB.38.3158**.
74 B. T. Thole and G. Van Der Laan, Systematics of the Relation between Spin-Orbit Splitting in the Valence Band and the Branching Ratio in X-Ray Absorption Spectra, *Europhys. Lett.*, 1987, **4**, 1083.
75 C. Cartier Dit Moulin, *et al.*, Spin Transition Evidenced by Soft X-Ray Absorption Spectroscopy, *J. Phys. Chem.*, 1992, **96**, 6196, DOI: **10.1021/j100194a021**.
76 S. Rohlf, *et al.*, Light-Induced Spin Crossover in an Fe(II) Low-Spin Complex Enabled by Surface Adsorption'', *J. Phys. Chem. Lett.*, 2018, **9**, 1491, DOI: **10.1021/acs.jpclett.8b00338**.
77 S. Rohlf, *et al.*, ''Influence of Substrate Electronic Properties on the Integrity and Functionality of an Adsorbed Fe(II) Spin-Crossover Compound'', *J. Phys. Chem. C*, 2019, **123**, 17774.
78 H. S. S. Decurtins, P. Gütlich and C. P. Kohler, ''Light Induced Excited Spin State Trapping in a Transition Metal Complex: The Hexa-1-Propyltetrazole-Iron (II) Tetrafluoroborate Spin-Crossover System'', *Chem. Phys. Lett.*, 1984, **105**, 1, DOI: **10.1016/0009-2614(84)80403-0**.
79 G. Chastanet, *et al.*, *Compr. Coord. Chem. II*, 2019, 1–19.
80 G. Chastanet, *et al.*, A Critical Review of the T(LIESST) Temperature in Spin Crossover Materials – What It Is and What It Is Not, *Chem. Squared*, 2018, 1.
81 V. Petrícek, *et al.*, Crystallographic Computing System JANA2006: General Features, *Zeitschrift fur Krist.*, 2014, **229**, 345, DOI: **10.1515/zkri-2014-1737**.
82 Z. Otwinowski, *et al.*, *Methods Enzymol.*, 1997, 307–326.
83 G. M. Sheldrick, SHELXT – Integrated Space-Group and Crystal-Structure Determination, *Acta Crystallogr., Sect. A: Found. Adv.*, 2015, **71**, 3, DOI: **10.1107/S2053273314026370**.
84 G. M. Sheldrick, Crystal Structure Refinement with SHELXL, *Acta Crystallogr. Sect. C Struct. Chem.*, 2015, **71**, 3, DOI: **10.1107/S2053229614024218**.
85 O. V. Dolomanov, *et al.*, OLEX2: A Complete Structure Solution, Refinement and Analysis Program, *J. Appl. Crystallogr.*, 2009, **42**, 339, DOI: **10.1107/S0021889808042726**.
86 O. Kahn, *Molecular Magnetism*, Wiley-VCH Verlag GmbH, Weinheim, 1993.
87 J. J. Yeh, *et al.*, Atomic Subshell Photoionization Cross Sections and Asymmetry Parameters: $1 \leqslant Z \leqslant 103$, *At. Data Nucl. Data Tables*, 1985, **32**, 1, DOI: **10.1016/0092-640X(85)90016-6**.
88 D. Nečas, *et al.*, Gwyddion: An Open-Source Software for SPM Data Analysis, *Open Phys.*, 2012, 10, DOI: **10.2478/s11534-011-0096-2**.
89 G. Poneti, *et al.*, Thermal and Optical Control of Electronic States in a Single Layer of Switchable Paramagnetic Molecules, *Chem. Sci.*, 2015, **6**, 2268, DOI: **10.1039/C5SC00163C**.